Infrared Spectropolarimetric Bidirectional Reflectance of LIDAR Targets and Building Materials—C.E. Mungan, Spring 2000

Introduction

Measurements of the reflectances of a variety of different lidar target samples and building construction materials have been performed under ambient conditions for a variety of incident and scattering angles in the near-infrared over all possible polarization states. This gives what is called the spectropolarimetric bidirectional reflectance. The target samples are of interest for laser radar calibrations, while the building materials are applicable to remote sensing applications. A Fourier-transform spectrometer (shown in Fig. 1) fitted with an external reflectance goniometer and with an incident and scattered polarization generator and analyzer, respectively, was used for this purpose at Eglin Air Force Base.

Fig. 1. Photograph of the Fourier transform interferometer at Eglin AFB.

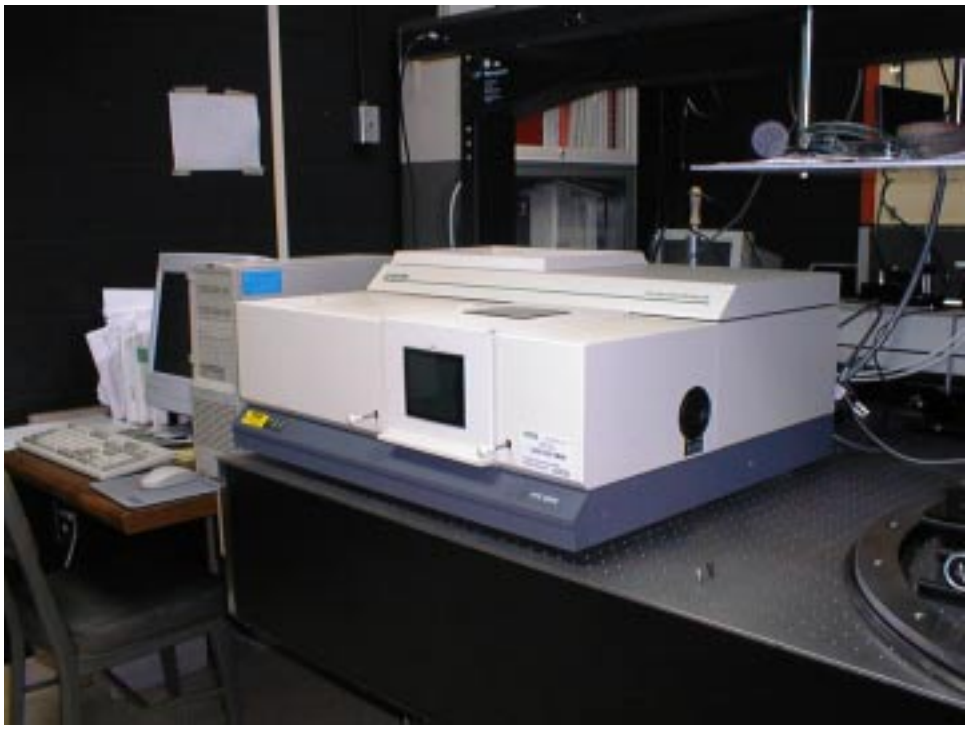

Experimental Setup

Fig. 2. Raw intensity spectrum of the source.

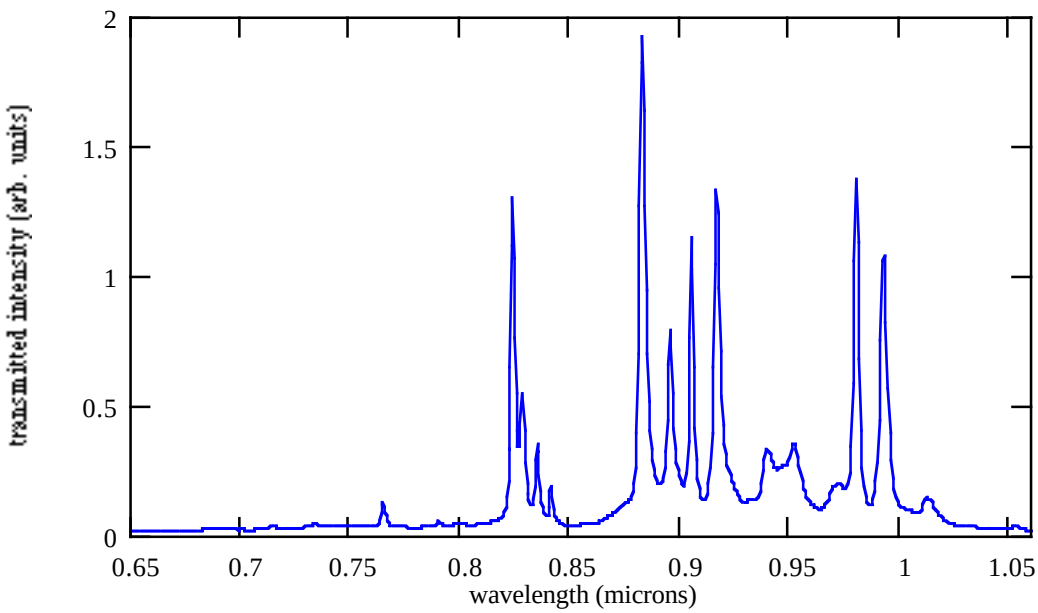

The Xe arc lamp spectrum in Fig. 2 shows discrete atomic emission lines, superimposed on top of a smooth thermal background. This blackbody background spectrum looks weak only because of the sharpness of the atomic lines; in fact, the thermal spectrum has enough strength for spectroscopy and the sharp lines are not of interest. In order to eliminate residual unratioed features at these strong lamp spectral peaks, the reflectance data were smoothed slightly.

The most general mapping of the bidirectional reflectance distribution function (BRDF) of a flat sample requires that four angles be continuously variable over the hemisphere about the sample's normal: the incident polar and azimuthal angles, θ_i and ϕ_i, and the reflected angles, θ_r and ϕ_r. These angles are sketched in Fig. 3. Note that the sample normal defines the *z*-axis, while the *x*-axis can be chosen to coincide with some preferred surface feature of the sample, such as striations, a crystallographic direction, or an optical axis. For an isotropic surface, having no such

preferred features, the BRDF is a function only of $\phi_r - \phi_i$ and not of the two azimuthal angles individually. The samples investigated in the present study are assumed to be isotropic when averaged over the area of illumination scattered into the detector aperture. Arbitrarily fixing ϕ_i at 0˚ by suitable choice of the coordinate system, this means that the BRDF only depends on ϕ_r.

Fig. 3. General geometry of the incident and reflected beams.

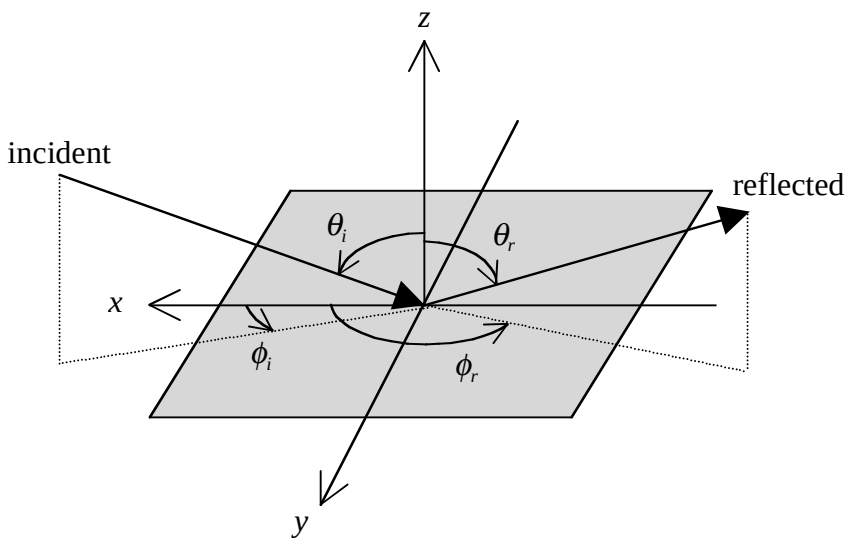

The spectropolarimetric reflectometer at Eglin AFB has the following geometry, as sketched in Fig. 4. The output retarder and polarizer, together with the mirror and detector, rotate around the sample on a motor-driven stage. The sample also rotates on an independently driven stage. A particular choice of the detector and sample positions fixes the incident and reflected polar angles. (Note carefully that the *z*-axis in Fig. 3 has been rotated by 90˚ in Fig. 4, so that rotations of the two stages determine the polar not the azimuthal angles.) In principle, out-of-plane azimuthal measurements can be performed by tilting the sample about the axis parallel to the optical bench in the plane of the sample. However, in the present work, only in-plane measurements (i.e., ϕ_r = 180˚) were made, in which the sample normal lies in the plane of the incident and reflected beams.

Fig. 4. Block diagram of the spectropolarimetric reflectometer.

Legend: A = attenuators, P = linear polarizer, R = achromatic retarder,

M = off-axis parabolic mirror, D = silicon detector.

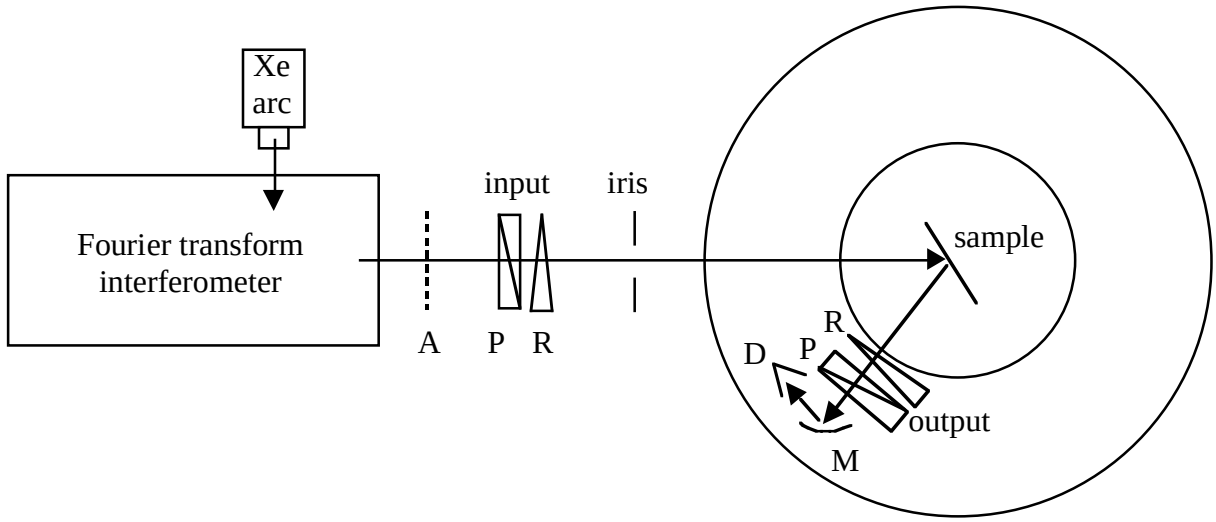

The device in Fig. 4 can be conceptually divided into three parts: a spectrometer, a polarimeter, and a reflectometer. The spectrometer modulates the radiation from the Xe arc source using a scanning Michelson-Morley interferometer with a quartz beamsplitter. The parameters for the spectrometer are as follows:

- speed of the scanning mirror = 5 kHz
- electronic filter = 5 kHz
- undersampling ratio = 1
- resolution = 16 cm^{-1}
- aperture = fully open
- number of scans to co-add = 64
- wavelength range = 0.65–1.06 μm

The modulated beam exits the spectrometer through its external port. Attenuators can be inserted or removed into this beam, as needed to limit the signal strength which ultimately falls on the detector to ±10 V. In addition, the sensitivity (which is an electronic gain) can be adjusted to boost weak signals; typically a sensitivity of 1 was used for the reference scans and a value of 16 for the sample scans.

The polarimeter consists of two matched pairs of polarizers and retarders. On the input side, the unpolarized incident beam first passes through a dichroic sheet linear polarizer, and the resulting linearly polarized beam next traverses an achromatic two-plate MgF_2 retarder, whose slow axis is delayed by a quarter wavelength compared to its fast axis. By rotating the optical axis of the retarder, it is possible to encode any desired elliptical polarization state into the harmonics of the intensity signal (Chenault *et al.*, 1998), i.e., with the major axis oriented at any desired angle, of either handedness, and with any desired ellipticity between 0 (circular) and 1 (linear). On the output side, the reflected beam passes through a matching polarizer-retarder combination in the opposite order. By suitably rotating the optical axis of the retarder, it is possible to transform any elliptical polarization state into a linearly polarized wave which can be analyzed by the linear polarizer. The polarimetric properties of a sample can be described in terms of its Mueller matrix, which is a 4×4 matrix $\mathbf{M}$ defining the transformation of the incident polarization state into the reflected polarization state—cf. Eq. (13) below.

Finally, the reflectometer consists of the rotating sample and detector stages. There are two ways of specifying the incident and reflected angles (cf. Fig. 5): either relative to the sample normal, or absolutely with respect to the optical bench. The former pair are the polar angles θ_i and θ_r defined previously in Fig. 3. By choice of our x-axis, θ_i is always positive. Taking ϕ_r to always be equal to 180˚ implies that θ_r is positive whenever the reflected beam lies on the other side of the sample normal than the incident beam, which is hereafter referred to as forward scattering. On the other hand, θ_r is taken to be negative for backward scattering, when the

incident and reflected beams both lie within the same *x*-*z* quadrant. Although this is contrary to the usual convention for the specification of polar angles, it simplifies the notation in the present work. The absolute angles θ_d and θ_s are measured with reference to the incident direction, using the convention that positive angles are measured in the clockwise direction and negative angles in the counter-clockwise direction. (This is not actually contrary to the standard convention for plane polar angles, because the incident beam points in the –*x* direction according to Fig. 3.) With these definitions, the conversion formulae from relative to absolute angles are

$$\begin{aligned} \theta_s &= -\theta_i \text{ and} \\ \theta_d &= 180^\circ - \theta_i - \theta_r . \end{aligned} \tag{1}$$

Fig. 5. Specification of the incident and reflected angles.

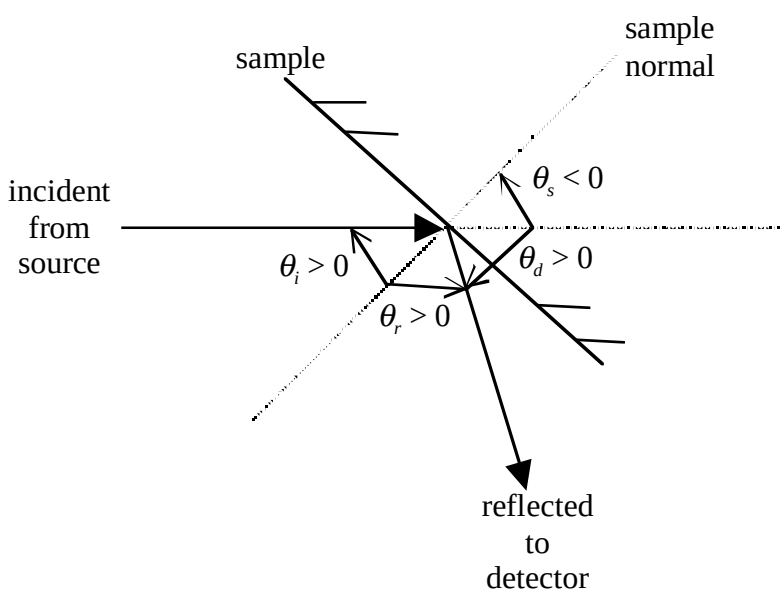

It is conventional in optics to employ the relative angles; for example, specular scattering corresponds to the case of $\theta_r = \theta_i$, while monostatic scattering (also referred to as backscattering) corresponds to $\theta_r = -\theta_i$, so called because in radar work it corresponds to using the same antenna both as the source and as the detector (as opposed to separate transmitting and receiving dishes for the bistatic case). However, it is simpler from the point of view of the experimental setup of Fig. 4 to use the absolute angles in practice. The absolute zero angle can be found for θ_d by peaking up the signal in the absence of a sample, and for θ_s by replacing the sample with a flat mirror and checking that the incident beam is reflected straight back toward the source.

Combining the spectrometer, polarimeter, and reflectometer components, it is evident that a data run consists of measuring a 4×4 array of spectra for each of a variety of different incident and reflected angles. Each data run is begun by collecting calibration data with no sample in place and with the detector looking straight back at the source through the spectrometer (i.e., $\theta_d = 0^\circ$). This generates both a background reference spectrum for determination of the reflectance, and error corrections for the retarders and polarizers. There are five possible errors, indicated as small angles ε in Fig. 6: discrepancies in the 90˚ retardances δ of the quarter-wave plates and orientation misalignments of the output polarization axis and of the retarder optical axes. (The input polarization axis is not crucial because the source beam is unpolarized and the polarizers remain fixed in orientation during the runs, in order to eliminate any possible polarization dependence of the optics either before the input polarizer or following the output polarizer.) Fortunately, the procedure for collecting the data and performing the Mueller matrix calculations is automated. Nevertheless, it requires large amounts of time, generally on the order of a couple of days per sample. A wealth of information can in principle be extracted from this large quantity of data.

Fig. 6. Polarization and retardation errors.

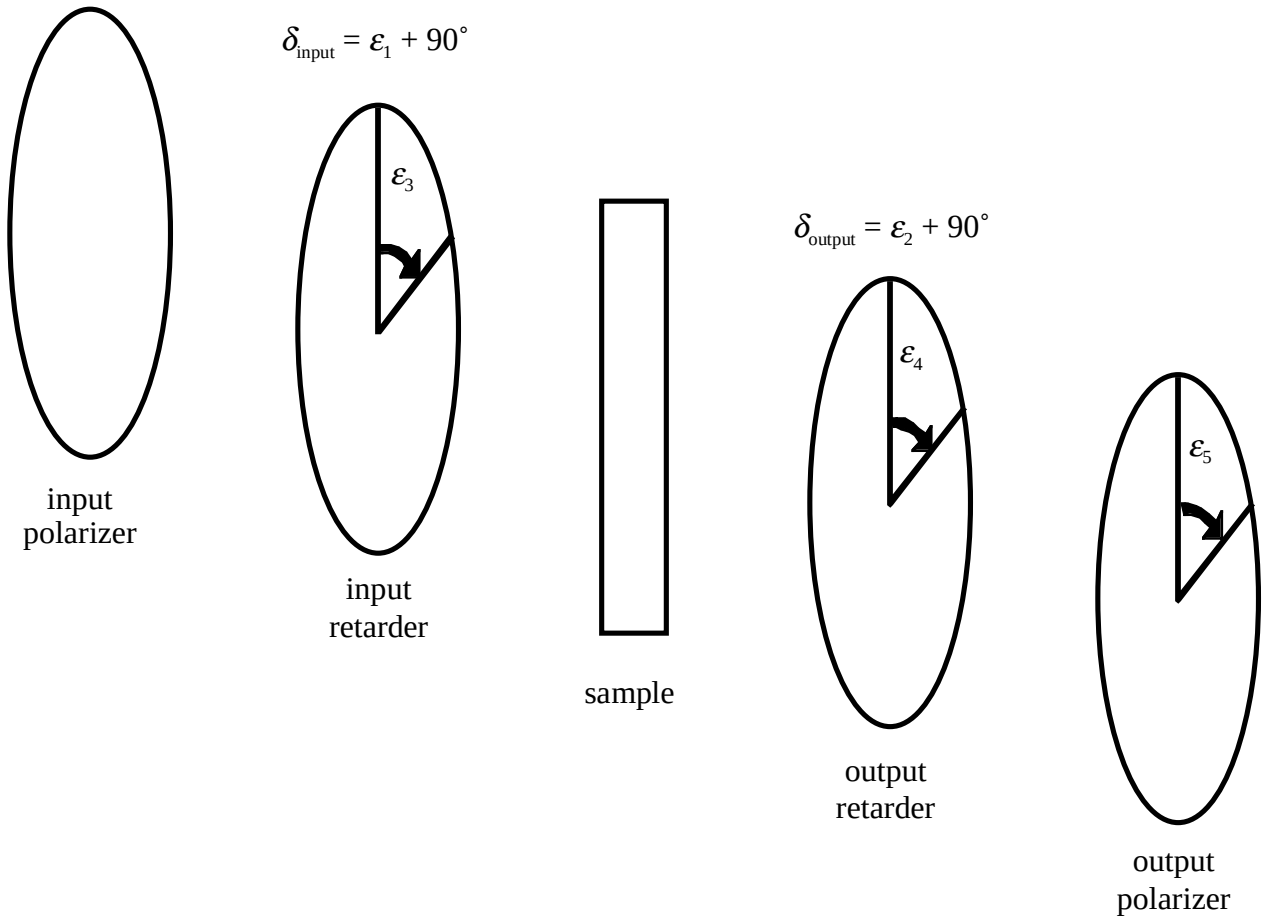

Thirteen samples were selected for study in the present work: six construction materials and seven lidar target board samples. They are all flat, square items measuring several inches on a side. A brief description of each is presented in Table 1 below.

Table 1. Description of samples studied.

Sample	Description
Construction Materials	
Foam	blue polystyrene housing insulation
Drywall	standard housing drywall material
Rubber	piece of soft black rubber
Wood	piece of standard plywood
Shingle	speckled grey roof shingle
Steel	steel plate painted military grey
LIDAR Target Boards	
2%	black paint
5%	black paint with slight sparkles
10%	black paint with more sparkles
A	grey paint with a sandpaper texture
B	grey-black paint with a sandpaper texture
E	grey-white paint with a sandpaper texture
Resolution	flat grey paint

In this report, the term "reflectance" always refer to the bidirectional reflectance, wherein light incident from one direction—within a narrow element of solid angle Ω_i defined by the iris—is reflected into some other direction—within a narrow element of solid angle Ω_r defined by the detector aperture. Dividing the bidirectional reflectance by the projected reflection solid angle, $\Omega_r \cos\theta_r$, gives the BRDF.

Theory of Polarized Light Scattering

The incident optical power P per unit illuminated area A of an object is known as the illuminance $H \equiv dP/dA$ in units of W/m^2; the corresponding scattered quantity is called the exitance. [Note that the element dA of area is taken to be small on the macroscopic scales of interest, but large compared to the sub-resolution irregularities in the sample surface, and is taken to be perpendicular to the macroscopic surface normal (Nicodemus, 1965).] When it is desired to speak of either the illuminance or the exitance, without specifying which, this report will refer to the irradiance of the surface. This is to be distinguished from the intensity of the irradiating beam, $I \equiv dP/(dA \cos\theta)$, where the $\cos\theta$ term projects the element of surface area dA into the direction of propagation of the beam, which is inclined at polar angle θ to the (macroscopic) surface normal. The irradiance per unit projected solid angle is called the radiance or luminance, which corresponds to the photometric concept of brightness, $L \equiv dH/(\cos\theta\, d\Omega) = dI/d\Omega$ in units of W/m^2/sr. Here the element of solid angle is $d\Omega \equiv \sin\theta\, d\theta\, d\phi$; sometimes (Nicodemus *et al.*, 1977) a separate symbol is also introduced for the element of projected solid angle $\cos\theta\, \mathrm{d}\Omega$, though I will not do so here. Let the subscript i refer to incident quantities and r to reflected (scattered) terms. The bidirectional reflectance distribution function (BRDF) can now be defined as

$$f(\theta_i,\phi_i;\theta_r,\phi_r) \equiv \frac{dL_r}{dH_i} = \frac{dP_r}{dP_i \cos\theta_r d\Omega_r} \tag{2}$$

with units of sr^{-1}; here dP_i is the incident power illuminating dA from direction (θ_i,ϕ_i) and dP_r is the radiant power reflected from dA into the outgoing solid angle $d\Omega_r$ centered about the direction (θ_r,ϕ_r). In the present work, all of the sample surfaces are macroscopically planar and the incident beam has a spatially uniform ("top hat") intensity profile, so that one can integrate Eq. (2) over a macroscopic area A of the sample to get

$$f(\theta_i;\theta_r,\phi_r-\phi_i)=\frac{dP_r}{P_i\cos\theta_r d\Omega_r} \tag{3}$$

where now P_i is the incident power illuminating A and dP_r is the flux reflected from A into $d\Omega_r$. Since the surfaces investigated here are taken to be isotropic, f is a function only of $\phi_r - \phi_i$ (which is fixed at 180˚ in this study) as explained previously. Unlike reflectances, which cannot exceed unity, the BRDF can be very large, becoming infinite for a purely specular reflector.

By integrating the BRDF over all scattered angles, one gets the dimensionless directional-hemispherical reflectance

$$\rho(\theta_i,\phi_i;2\pi)=\int_{2\pi} f(\theta_i,\phi_i;\theta_r,\phi_r)\cos\theta_r d\Omega_r\,, \tag{4}$$

which gives the fractional amount of power reflected into the entire hemisphere out of that incident from a particular direction. (The integral over 2π is a shorthand meaning integrate θ from 0 to $\pi/2$ and ϕ from 0 to 2π, for a total solid angle of 2π.) If instead one averages over all incident angles, the hemispherical-directional reflectance is obtained as

$$d\rho(2\pi;\theta_r,\phi_r)=\frac{\cos\theta_r d\Omega_r}{\pi}\int_{2\pi} f(\theta_i,\phi_i;\theta_r,\phi_r)\cos\theta_i d\Omega_i\,. \tag{5}$$

Note that the denominator is π and not 2π because of the $\cos\theta_i$ projection factor. In the spirit of Eqs. (4) and (5), the bihemispherical reflectance (or albedo) is given by

$$\rho(2\pi;2\pi)=\frac{1}{\pi}\iint_{2\pi} f(\theta_i,\phi_i;\theta_r,\phi_r)\cos\theta_i d\Omega_i\cos\theta_r d\Omega_r\,. \tag{6}$$

Other similar quantities, such as the conical-hemispherical reflectance, have been tabulated by Judd (1967) and by Nicodemus *et al.* (1977). If the prefactor before the integral in Eq. (5) is left off, the resulting quantity is instead called the hemispherical-directional reflectance factor, which is defined as the ratio of the flux reflected by the sample to that which would be reflected by an ideal Lambertian reflector for the same geometry, because $f = 1/\pi$ for the latter (Mungan, 1998).

From the definition of the BRDF, the scattered radiance can be related to the incident radiance by

$$L_r(\theta_r,\phi_r) = \int_{\Omega_i} L_i(\theta_i,\phi_i)\, f(\theta_i,\phi_i;\theta_r,\phi_r)\cos\theta_i d\Omega_i\,, \tag{7}$$

which can be rather complicated to evaluate analytically. The emissivity is given by Kirchhoff's law as

$$\varepsilon(\theta_i,\phi_i) = 1 - \int_{2\pi} f(\theta_i,\phi_i;\theta_r,\phi_r)\cos\theta_r d\Omega_r \tag{8}$$

and is thus determined by the BRDF. Hence a separate measurement of the emissivity is not required.

According to the Helmholtz reciprocity theorem, $f(\theta_i,\phi_i;\theta_r,\phi_r) = f(\theta_r,\phi_r;\theta_i,\phi_i)$, so that either direction may be that of the incident beam with the other the reflected beam. Note from Eqs. (4) and (5) that this would imply that the directional-hemispherical reflectance equals the hemispherical-directional reflectance factor; interestingly enough, however, equality of these two reflectance terms remains true even when Helmholtz reciprocity does not (Nicodemus, 1970). There has been considerable discussion about the conditions under which reciprocity holds (Clarke and Parry, 1985; Kriebel, 1996; Shirley *et al.*, 1997; Snyder, 1998)—for example, it clearly does not apply to a Faraday isolator. It is generally accepted however that the theorem is obeyed by most materials (including compound objects) under ordinary conditions and hence models which are not reciprocal are generally considered unphysical and experimental failures

are often attributed to measurement errors or limitations.

Equation (3) contains no polarization information and relates only the total incident and reflected optical fluxes to each other. In order to quantify the polarimetric scattering, we need to retain the phase information about the electric fields associated with the beams and not simply their intensities. There are two alternative representations for doing so (Hecht, 1998). The Jones calculus writes each electric field as a vector of two complex components, and the scattering is then described by a 2×2 matrix. This formalism is not applicable to the present work, as it implicitly assumes that each beam is fully polarized and coherent. To instead handle incoherent light which is partially polarized in general, as we need here, each beam can be represented by a column vector of four real components. This vector is called the Stokes vector **S** and its four components are called the Stokes parameters $\{S_0,S_1,S_2,S_3\}$. These parameters can be defined either operationally or from electromagnetic theory. To get the former, imagine a set of three ideal polarizers, i.e., they perfectly transmit a specific polarization state and perfectly block the complementary polarization state. (That is, their diattenuations, as defined below, for the appropriate polarization states are 100%.) Note that each polarizer therefore transmits half of the intensity of incident unpolarized light. Filter 1 is a linear polarizer whose pass axis is horizontal; filter 2 is another linear polarizer but with a pass axis inclined at +45˚; and filter 3 is a right-handed circular polarizer. (For the present case of surface scattering, these axes are defined relative to the plane of incidence or reflection, as appropriate. That is, horizontal means *s*-polarized and vertical means *p*-polarized.) Let I_0 be the incident beam intensity, and denote the intensities transmitted by each polarizer as I_1, I_2, and I_3, respectively. Then the normalized Stokes parameters are given by

$$\begin{aligned} S_0 &= 1 \\ S_1 &= 2I_1 / I_0 - 1 \\ S_2 &= 2I_2 / I_0 - 1 \\ S_3 &= 2I_3 / I_0 - 1 \end{aligned} \tag{9}$$

so that S_1, S_2, and S_3 each vary between –1 and +1 and specify the state of polarization: $S_1 > 0$ means the beam is preferentially horizontally (H) polarized, while $S_1 < 0$ indicates it is predominantly vertically (V) polarized; S_2 refers to the tendency to be linearly polarized at +45˚ ($S_2 > 0$) or –45˚ ($S_2 < 0$); and finally S_3 indicates preferential right-handed circular (RHC) versus left-handed circular (LHC) polarizations by its sign. If the normalized Stokes vector is multiplied by the total beam intensity, then the unnormalized Stokes vector (denoted by a tilde) results,

$$\tilde{\mathbf{S}} = I_0 \mathbf{S} \tag{10}$$

so that $\tilde{S}_0 = I_0$. Alternatively, from an electromagnetic point of view, if the complex amplitude of an electric field vector is written as $(E_{0x}e^{i\varphi_x}, E_{0y}e^{i\varphi_y})$, then

$$\begin{aligned} S_1 &= \left\langle E_{0x}^2 - E_{0y}^2 \right\rangle \Big/ \left\langle E_{0x}^2 + E_{0y}^2 \right\rangle \\ S_2 &= \left\langle 2E_{0x}E_{0y}\cos\varphi \right\rangle \Big/ \left\langle E_{0x}^2 + E_{0y}^2 \right\rangle \\ S_3 &= \left\langle 2E_{0x}E_{0y}\sin\varphi \right\rangle \Big/ \left\langle E_{0x}^2 + E_{0y}^2 \right\rangle \end{aligned} \tag{11}$$

where $\varphi \equiv \varphi_y - \varphi_x$ and the angular brackets denote time averages. From this we see that if the beam is unpolarized, then $\left\langle E_{0x}^2 \right\rangle = \left\langle E_{0y}^2 \right\rangle$ and $\langle \varphi \rangle = 0$ independently of the real amplitudes, so that $S_1 = S_2 = S_3 = 0$. At the other extreme, for fully polarized light Eq. (11) implies that $S_1^2 + S_2^2 + S_3^2 = 1$. In general, the degree of polarization of a beam is defined as

$$DOP \equiv \frac{I_{pol}}{I_0} = \frac{\sqrt{\tilde{S}_1^2 + \tilde{S}_2^2 + \tilde{S}_3^2}}{\tilde{S}_0} = \sqrt{S_1^2 + S_2^2 + S_3^2}\,, \tag{12}$$

where the total intensity I_0 is equal to the sum of its polarized portion, I_{pol}, and its unpolarized portion, I_{unpol}. For example, $DOP = 0$ for an unpolarized beam, while $DOP = 1$ for fully polarized light.

Now, the incident and reflected beams are related by a 4×4 matrix called the unnormalized Mueller matrix,

$$\tilde{\mathbf{S}}_r = \tilde{\mathbf{M}}\tilde{\mathbf{S}}_i \tag{13a}$$

which we can write out explicitly in component form using Eq. (10) as

$$\begin{bmatrix} I_{0r} \\ \tilde{S}_{1r} \\ \tilde{S}_{2r} \\ \tilde{S}_{3r} \end{bmatrix} = \begin{bmatrix} \tilde{M}_{00} & \tilde{M}_{01} & \tilde{M}_{02} & \tilde{M}_{03} \\ \tilde{M}_{10} & \tilde{M}_{11} & \tilde{M}_{12} & \tilde{M}_{13} \\ \tilde{M}_{20} & \tilde{M}_{21} & \tilde{M}_{22} & \tilde{M}_{23} \\ \tilde{M}_{30} & \tilde{M}_{31} & \tilde{M}_{32} & \tilde{M}_{33} \end{bmatrix} \begin{bmatrix} I_{0i} \\ \tilde{S}_{1i} \\ \tilde{S}_{2i} \\ \tilde{S}_{3i} \end{bmatrix}. \tag{13b}$$

Comparing this to Eq. (2), we see that for incident and reflected unpolarized beams,

$$\tilde{M}_{00} = f(\theta_i, \phi_i; \theta_r, \phi_r) \cos\theta_r d\Omega_r, \tag{14}$$

i.e., the top leftmost element of the unnormalized Mueller matrix is equal to the bidirectional reflectance. The other elements in the matrix give polarimetric information. Thus, the Mueller matrix can be thought of as a generalization of the BRDF to polarized scattering (Flynn and Alexander, 1995). It is conventional to normalize the Mueller matrix by ratioing out the unpolarized reflectance,

$$\mathbf{M} \equiv \tilde{\mathbf{M}} / \tilde{M}_{00}. \tag{15}$$

From this normalized Mueller matrix, all polarization properties of interest can be calculated. For example, if unpolarized light is incident on the sample, then Eq. (13b) becomes

$$\begin{bmatrix} \tilde{S}_{0r} \\ \tilde{S}_{1r} \\ \tilde{S}_{2r} \\ \tilde{S}_{3r} \end{bmatrix} = \begin{bmatrix} \tilde{M}_{00} & \tilde{M}_{01} & \tilde{M}_{02} & \tilde{M}_{03} \\ \tilde{M}_{10} & \tilde{M}_{11} & \tilde{M}_{12} & \tilde{M}_{13} \\ \tilde{M}_{20} & \tilde{M}_{21} & \tilde{M}_{22} & \tilde{M}_{23} \\ \tilde{M}_{30} & \tilde{M}_{31} & \tilde{M}_{32} & \tilde{M}_{33} \end{bmatrix} \begin{bmatrix} I_{0i} \\ 0 \\ 0 \\ 0 \end{bmatrix} = I_{0i} \begin{bmatrix} \tilde{M}_{00} \\ \tilde{M}_{10} \\ \tilde{M}_{20} \\ \tilde{M}_{30} \end{bmatrix} \tag{16}$$

so that the scattered beam is in general polarized. The degree of polarization of the reflected beam for an unpolarized incident beam defines the polarizance, P (Sornsin and Chipman, 1996). Using Eq. (12), this is seen to be

$$P = \frac{\sqrt{(I_{0i}\tilde{M}_{10})^2 + (I_{0i}\tilde{M}_{20})^2 + (I_{0i}\tilde{M}_{30})^2}}{I_{0i}\tilde{M}_{00}} = \sqrt{M_{10}^2 + M_{20}^2 + M_{30}^2} \tag{17}$$

and is thus determined by the first column of the Mueller matrix. It is a fraction varying between 0 and 1, and is thus conveniently expressed as a percentage. For example, $P = 1$ for an ideal

polarizer, while $P = 0$ for an ideal retarder. An ideal polarizer, as previously mentioned, fully passes one polarization state while completely blocking the complementary polarization state. This is described by a quantity called the diattenuation, D, that quantifies variations in the scattered power as a function of the incident polarization state. The diattenuation vector **D** has three components, each of which can vary from –1 to +1: $D_1 = M_{01}$ which describes H–V diattenuation, $D_2 = M_{02}$ which describes ±45˚ diattenuation, and $D_3 = M_{03}$ which describes RHC–LHC diattenuation. The overall magnitude of this vector is

$$D = \sqrt{M_{01}^2 + M_{02}^2 + M_{03}^2}\,, \tag{18}$$

determined by the first row of the Mueller matrix. Like P, it is a fraction conveniently expressed as a percentage between 0 and 100%.

In studying the polarimetry of materials, an important question is the extent to which the polarization state of a beam is preserved by the interaction with the sample or device. This is described by the general concept of "depolarization." Unfortunately, two distinct definitions of depolarization are used in the literature. To avoid this confusion, I will here coin two alternate names for these processes. On the one hand, one can ask for the degree to which a polarized beam becomes unpolarized; this will be called the unpolarizance, U. On the other hand, one can ask about changes from one state to another state of polarization; let's term this the transpolarizance. For example, suppose an s-polarized beam is incident on some device or material, and the exiting beam is 10% s, 20% p, 40% RHC, and 30% unpolarized. Then we would say that the s-unpolarizance is 30% and the s-transpolarizance is 60%. A measure of the unpolarizance is given by (Sornsin and Chipman, 1996)

$$U = 1 - \sqrt{\frac{\left(\sum_{i,j=0}^{3} M_{ij}^2\right) - 1}{3}}\,, \tag{19}$$

expressed as a percentage between 0 and 100%. If $U = 0$, then the exiting light is fully polarized

for any incident polarization state; this occurs when $\left\langle M_i^2 \right\rangle = 1$, where $\mathbf{M}_i$ is the ith row vector of the Mueller matrix and the average is over all four rows. For example, $U = 0$ for an ideal polarizer or retarder. Note that since the sum of M_{ij}^2 equals the trace of **M** multiplied by its transpose, this definition is equivalent to Eq. (29) of Kim *et al.* (1987).

If a material does not unpolarize light, then its Mueller matrix can be uniquely decomposed into the product of a diattenuating component and a retarding component (Chenault *et al.*, 1998). While the diattenuation vector **D** measures the relative changes in the real amplitudes of the scattered electric field components for complementary polarization states, the retardance vector **R** measures the relative changes in their phases. The overall magnitude of the retardance is given by a fairly involved expression,

$$R = \cos^{-1}\left[\frac{\left(\sum_{i=1}^{3} M_{ii}\right) - \left(\sum_{i=1}^{3} M_{i0}M_{0i}\right) \Big/ \left(1+\sqrt{1-D^2}\right)}{2\sqrt{1-D^2}} - 0.5\right] \tag{20}$$

which can vary between 0 and 180˚. For example, this expression gives $R = 90^\circ$ for a quarter-wave plate for any orientation of its fast axis, but an indeterminate answer for any ideal polarizer, as expected because the complex number $z = 0$ has an undefined phase angle.

Experimental Results

The data for the polarizance, diattenuation, retardance, and unpolarizance were found for all samples to be relatively constant over the 800–1000 nm spectral range. Consequently they were averaged over this interval and are reported in the following tables.

In Table 2, three pairs of angles are specular, $\theta_i = \theta_r$. In Table 3, as in many cases, most angles were chosen to correspond to forward scattering, for which interesting polarimetric behavior is expected.

Table 2. Averaged results for the 2% lidar target sample.

θ_i	θ_r	P	D	R	U
45˚	45˚	73.5%	69.8%	92.9˚	15.1%
75˚	75˚	40.7%	41.5%	89.7˚	6.2%
75˚	0˚	54.4%	64.9%	111.8˚	12.6%
20˚	20˚	15.0%	16.1%	90.2˚	7.7%
45˚	75˚	77.8%	77.5%	93.7˚	13.0%

Table 3. Averaged results for the 5% lidar target sample.

θ_i	θ_r	P	D	R	U
45˚	45˚	47.1%	48.8%	100.0˚	34.1%
75˚	75˚	38.0%	37.6%	87.2˚	6.5%
45˚	75˚	66.6%	66.9%	93.0˚	20.4%

Table 4. Averaged results for the 10% lidar target sample.

θ_i	θ_r	P	D	R	U
45˚	45˚	31.9%	31.7%	93.1˚	17.7%
75˚	75˚	43.5%	43.7%	89.6˚	14.4%
75˚	0˚	57.7%	62.4%	119.4˚	–
0˚	75˚	16.8%	34.8%	111.3˚	12.5%
20˚	20˚	5.7%	5.8%	93.4˚	8.7%

In Table 4, the 75˚–0˚ data afford a test of reciprocity, wherein the incident and reflected beams are swapped. Note however from Eq. (14) that this requires a correction for the projection factor and has not been pursued in this report. The dash indicates a small value, but the data were too noisy to permit a reliable determination of it.

Table 5. Averaged results for lidar target sample A.

θ_i	θ_r	P	D	R	U
45˚	45˚	18.3%	18.0%	113.1˚	76.6%
45˚	75˚	39.2%	40.3%	107.1˚	56.4%
20˚	20˚	2.7%	3.8%	116.8˚	85.6%

Note in Table 5 how large the unpolarizance values are. As discussed in connection with Eq. (20), this renders the determinations of the retardance questionable.

Table 6. Averaged results for lidar target sample B.

θ_i	θ_r	P	D	R	U
45˚	45˚	45.8%	46.3%	104.8˚	43.4%
75˚	75˚	54.2%	54.4%	89.6˚	6.3%
60˚	0˚	34.3%	26.8%	116.7˚	30.1%

Note in Table 6, as is the case for most of the samples, that the retardance is about 100˚ for any pair of angles.

Table 7. Averaged results for lidar target sample E.

θ_i	θ_r	P	D	R	U
45˚	45˚	4.5%	4.3%	137.0˚	34.5%
45˚	25˚	2.4%	2.4%	137.1˚	38.9%
45˚	75˚	14.5%	17.1%	90.4˚	3.5%
20˚	20˚	2.2%	11.3%	103.5˚	44.1%
75˚	45˚	10.1%	18.4%	95.5˚	12.5%
75˚	60˚	13.8%	22.2%	94.8˚	–
75˚	75˚	18.1%	26.3%	95.4˚	–
45˚	45˚	4.7%	4.4%	100.3˚	32.1%
75˚	–45˚	0.7%	0.7%	106.3˚	44.9%
75˚	75˚	19.2%	18.9%	93.1˚	28.5%
75˚	85˚	22.3%	22.2%	91.4˚	22.8%

Two sets of runs in Table 7 were repeated many months apart, after the spectropolarimeter had been moved to a new lab and realigned from scratch, resulting in a substantial improvement in signal-to-noise for the later runs below the double line. In view of this, the reproducibility of the data is seen to be fairly good in these two cases. One might thus reasonably expect self-consistency among the runs for the other samples, which were collected as a set either with the old or the new setup.

Table 8. Averaged results for the resolution board sample.

θ_i	θ_r	P	D	R	U
45˚	45˚	83.4%	85.4%	90.5˚	2.5%
75˚	75˚	48.2%	50.2%	88.1˚	1.4%
75˚	0˚	1.1%	11.5%	117.4˚	86.8%
20˚	20˚	16.6%	17.0%	93.8˚	10.6%

Note the surprisingly large range of values for *P*, *D*, and *U* in Table 8.

Table 9. Averaged results for the construction samples for $\theta_i = \theta_r = 45˚$.

Sample	P	D	R	U
foam	54.7%	67.9%	101.3˚	25.9%
wood	17.0%	20.8%	113.7˚	72.3%
drywall	19.4%	24.7%	112.3˚	72.2%
rubber	68.7%	80.9%	88.7˚	12.3%
shingle	11.5%	16.2%	116.3˚	83.3%
steel	58.5%	69.3%	92.1˚	18.8%

It is easier to understand these data visually. A number of different graphs are possible and presented below.

Fig. 7. Lidar target samples at $\theta_i = 45^\circ$ and $\theta_r = 45^\circ$.

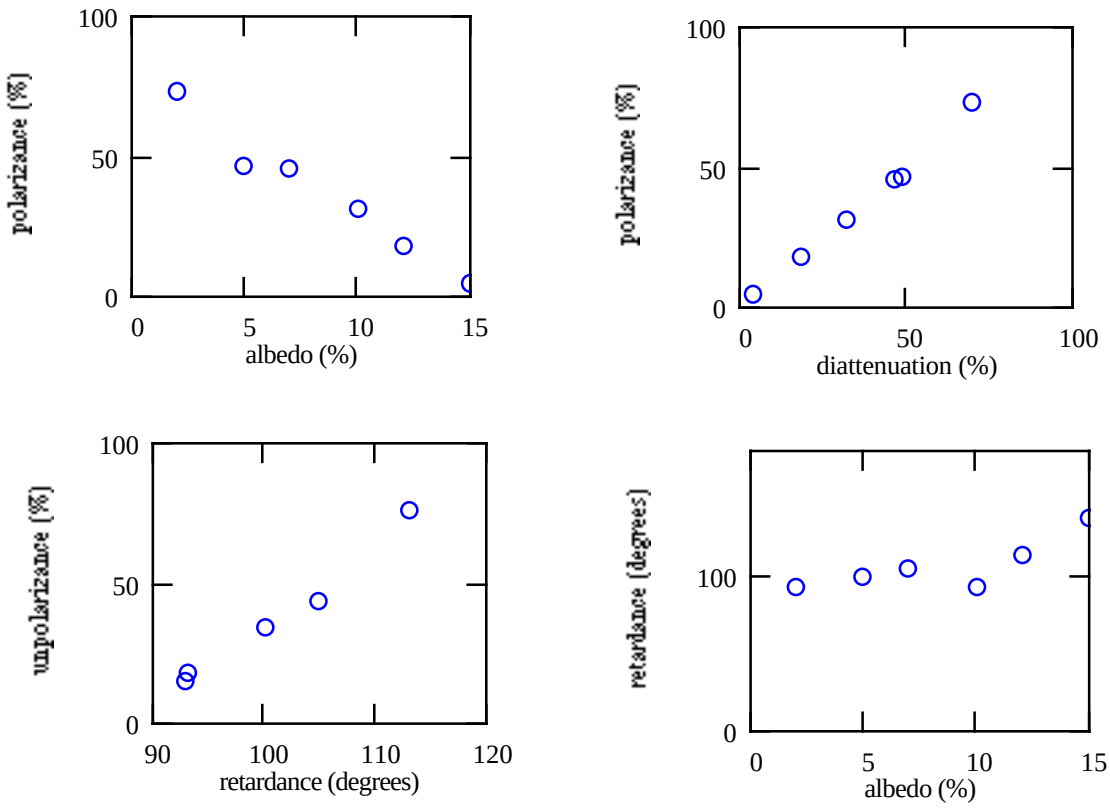

In Fig. 7, I have plotted the averaged data for the lidar samples for the important case of 45˚ specular scattering. The albedos are estimated from their nominal ratings or visual appearances, as listed in Table 10.

We see from the top left graph in Fig. 7 that the polarizance decreases with the reflectance. More highly absorbing samples polarize the light more efficiently. The explanation for this is the well-known fact that the reflectance of *p*-polarized light is lower than that of *s*-polarized light at any oblique angle (Hecht, 1998). In particular, the former equals zero at the Brewster angle for a

dielectric medium such as the paint coating on the samples. (Even for metal surfaces, the *p*-reflectance has a minimum, albeit not a zero, at the pseudo-Brewster angle.) Thus, as the sample absorptance increases, and hence the reflectance decreases (since the reflectance and absorptance sum to unity for an opaque sample), only the *s*-polarized beam survives. The top right graph in Fig. 7 shows that the polarizance is strongly linearly correlated to the diattenuation, confirming this conclusion.

In the lower right graph in Fig. 7, it can be seen that the retardance hovers around 90˚ at low sample reflectances, but rises at larger reflectances. In fact, perfect mirror-like reflection can be obtained for a real surface at 180˚ forward scattering (i.e., specular scattering at grazing incidence), whether a dielectric or a conductor. We might then be tempted to predict a simple 180˚ phase shift upon reflection from a high albedo sample for any polarization state, following a consideration of the electromagnetic boundary conditions for grazing scattering (Hecht, 1998). However, this line of reasoning can be seen to be incorrect by examining the lower left graph in Fig. 7: at high retardances, the samples unpolarize an incident beam, in striking contradistinction to the effect of a mirror. At high albedos, our samples become perfect diffuse not specular reflectors, i.e., they are more nearly Lambertian than mirror-like and hence it is no surprise that the scattered light is unpolarized.

Table 10. Estimated bihemispherical reflectances of the lidar samples.

Target Sample	Estimated Albedo
2%	2%
5%	5%
B	7%
10%	10%
A	12%
E	15%

Fig. 8. Construction samples at $\theta_i = 45^\circ$ and $\theta_r = 45^\circ$.

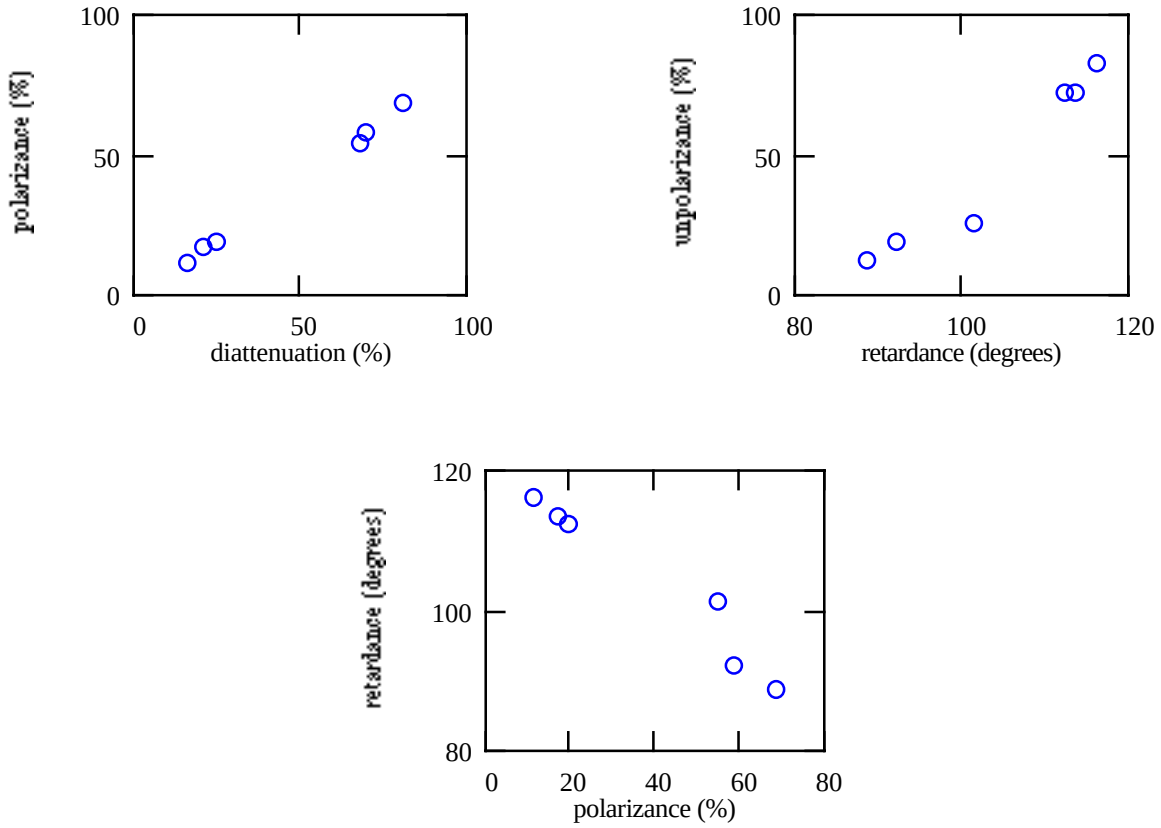

Figure 8 presents results for the construction materials at 45˚ specular scattering. The upper two graphs are similar in their trends to the corresponding graphs in Fig. 7. Since it is difficult to estimate the albedos for these samples, the other two graphs in Fig. 7 have been combined into the lower graph in Fig. 8. The retardance appears to approach 90˚ as the polarizance and hence the diattenuation rises toward 100%. An average retardance of 90˚ can result if the *p*-component of the scattered light has a 0˚ phase shift while the *s*-component has a 180˚ shift, as is true for specular reflection from a dielectric at angles of incidence below the Brewster angle (Hecht, 1998).

Figure 9 plots target sample E for three different cases of specular reflection, $\theta_i = \theta_r$.

Fig. 9. Lidar sample E for specular scattering.

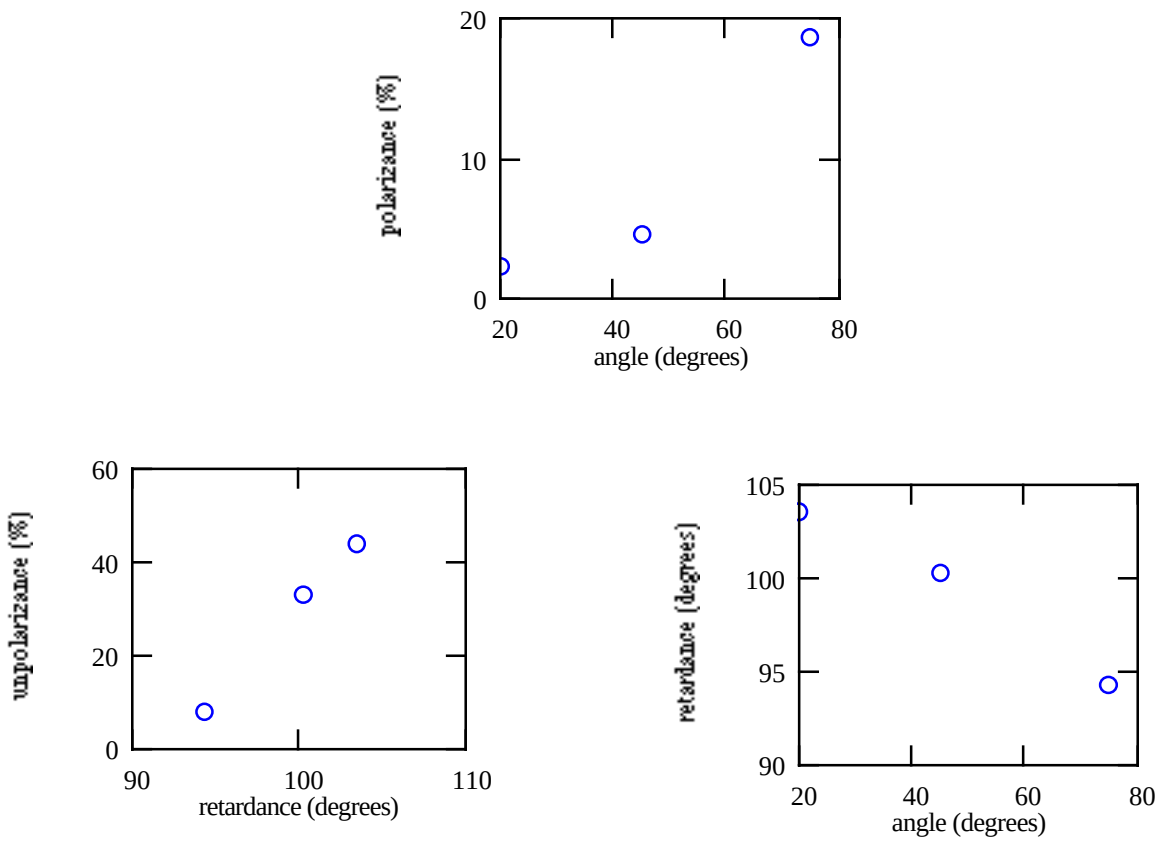

The top graph in Fig. 9 implies that the polarizance rises with the specular angle. This suggests a rather high Brewster angle and hence real part of the index of refraction of the surface, just as the glare off the surface of a lake is preferentially horizontally polarized. Surprisingly, the retardance is seen in the lower right graph in Fig. 9 to decrease with the scattering angle, in contrast to the 180˚ phase shift expected for a mirror.

Similar behavior is observed for specular scattering from the 2%, 10%, and resolution board lidar samples. On the other hand, Fig. 10 shows what happens if we fix the angle of incidence at 45˚ and allow the angle of reflection to sweep through the specular direction.

Fig. 10. Lidar sample E at $\theta_i = 45^\circ$.

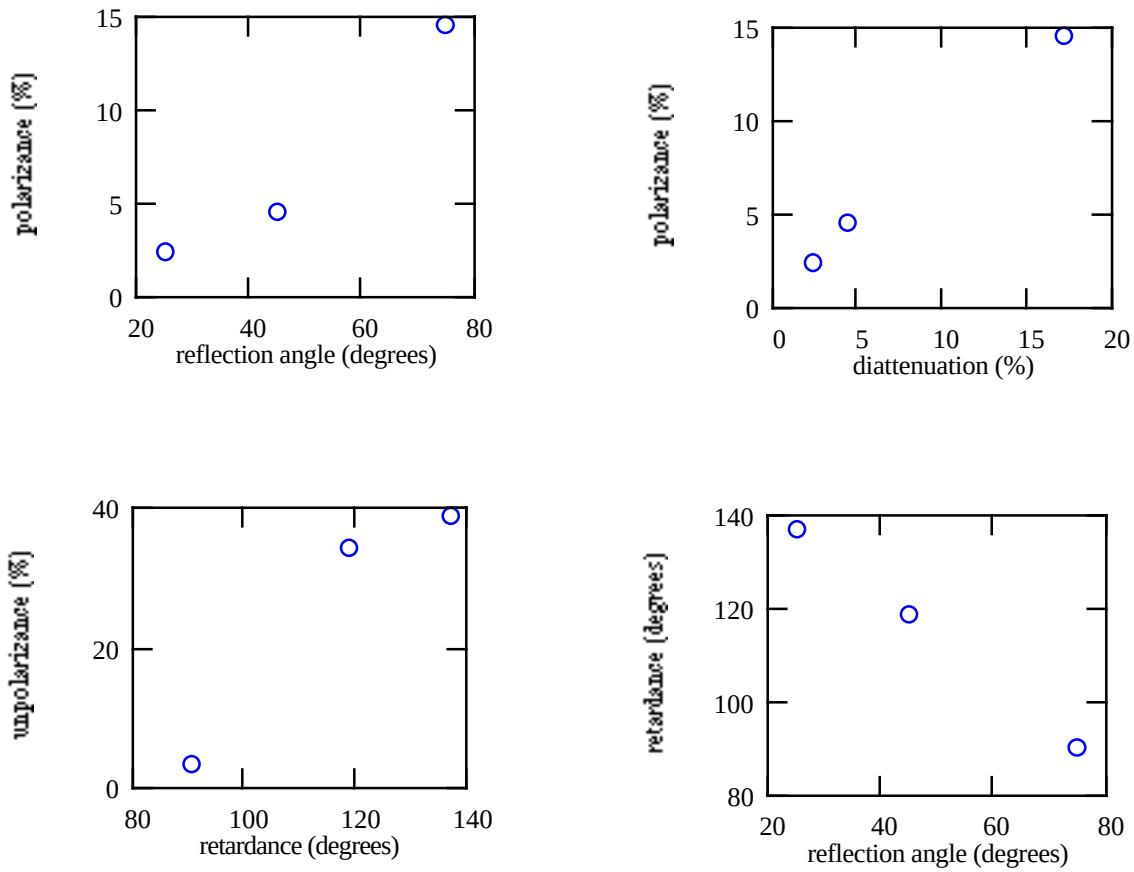

The polarizance increases as θ_r moves toward grazing, and correspondingly the diattenuation rises in step. The lower two plots in Fig. 10 resemble those of Fig. 9, indicating that the polarimetric dependence of the specular and off-specular beams are very similar, which is perhaps not surprising for diffuse scattering. Similar, although noisier, results are found for $\theta_i = 75^\circ$. In further confirmation of this, the lidar target samples for $\theta_i = 45^\circ$ and $\theta_r = 75^\circ$ give graphs like those of Fig. 7.

References

D.B. Chenault, D.H. Goldstein, and D.M Hayes (1998), "Fourier transform spectropolarimetry for optical diagnostics of transmissive materials," SPIE Proc. **3425**, 258.

F.J.J. Clarke and D.J. Parry (1985), "Helmholtz reciprocity: Its validity and application to reflectometry," Light. Res. & Tech. **17**, 1.

D.S. Flynn and C. Alexander (1995), "Polarized surface scattering expressed in terms of a bidirectional reflectance distribution function matrix," Opt. Eng. **34**, 1646.

E. Hecht (1998), "Optics," 3rd ed. (Addison-Wesley, Reading MA).

D.B. Judd (1967), "Terms, definitions, and symbols in reflectometry," J. Opt. Soc. Am. **57**, 445.

K. Kim, L. Mandel, and E. Wolf (1987), "Relationship between Jones and Mueller matrices for random media," J. Opt. Soc. Am. A **4**, 433.

K.-T. Kriebel (1996), "On the limited validity of reciprocity in measured BRDFs," Remote Sens. Environ. **58**, 52.

C.E. Mungan, (1998), "Bidirectional reflectance distribution functions describing first-surface scattering," AFOSR Final Report for the Summer Faculty Research Program.

F.E. Nicodemus (1965), "Directional reflectance and emissivity of an opaque surface," Appl. Opt. **4**, 767.

F.E. Nicodemus (1970), "Reflectance nomenclature and directional reflectance and emissivity," Appl. Opt. **9**, 1474.

F.E. Nicodemus, J.C. Richmond, J.J. Hsia, I.W. Ginsberg, and T. Limperis (1977), "Geometrical considerations and nomenclature for reflectance," NBS Monograph 160.

P. Shirley, H. Hu, B. Smits, E. Lafortune (1997), "A practitioners' assessment of light reflection models," Proceedings of the Pacific Graphics Conference.

W.C. Snyder (1998), "Reciprocity of the bidirectional reflectance distribution function (BRDF) in measurements and models of structured surfaces," IEEE Trans. Geosci. Remote Sensing **36**, 685.

E.A. Sornsin and R.A. Chipman (1996), "Polarization BRDF of satellite materials," Proceedings of the Workshop on Infrared and Millimeter Wave Polarimetry.